Increasing the efficiency of paleointensity analyses by selection of samples using first-order reversal curve diagrams

Claire Carvallo, Andrew P. Roberts, Roman Leonhardt, Carlo Laj, Catherine Kissel, Mireille M. Perrin, Pierre Camps

Increasing the efficiency of paleointensity analyses by selection of samples using first-order reversal curve diagrams

Claire Carvallo,[1,2] Andrew P. Roberts,[1] Roman Leonhardt,[3] Carlo Laj,[4] Catherine Kissel,[4] Mireille Perrin,[5] and Pierre Camps[5]

Received 27 October 2005; revised 27 June 2006; accepted 16 August 2006; published 14 December 2006.

[1] The global paleointensity database is restricted by the high failure rate of paleointensity analyses. Excluding thermal alteration, failure is usually caused by the presence of multidomain grains and interactions among grains, two properties that can be identified using first-order reversal curve (FORC) diagrams. We measured FORC diagrams on sister samples of about 200 samples that had been used for Thellier paleointensity determinations and determined criteria to discriminate samples that gave acceptable paleointensity results from those that did not. The three most discriminating criteria are the vertical spread of the FORC distribution (indicative of interactions), expressed as the full width at half maximum (FWHM), the spread of the FORC distribution along the $H_c = 0$ axis (width), and the bulk coercivity H_c (both indicative of domain state). Setting thresholds at 132 mT for the width of the distribution and 29 mT for the FWHM maximizes the number of unsuccessful rejected samples. Using an additional threshold of $H_c = 5.4$ mT results in rejection of 32% of unsuccessful samples. Seven samples that barely satisfy the paleointensity selection criteria would also be rejected using these selection criteria. Most of the samples that fail the paleointensity experiment without being detected by our selection criteria have ideal noninteracting single-domain magnetic properties but fail because of the thermal alteration that results from repeated heating. Being able to eliminate at least one third of unsuccessful samples using our FORC diagram-based prescreening procedure should provide a significant improvement in efficiency of paleointensity measurements.

Citation: Carvallo, C., A. P. Roberts, R. Leonhardt, C. Laj, C. Kissel, M. Perrin, and P. Camps (2006), Increasing the efficiency of paleointensity analyses by selection of samples using first-order reversal curve diagrams, *J. Geophys. Res.*, *111*, B12103, doi:10.1029/2005JB004126.

1. Introduction

[2] Estimating the ancient intensity of the geomagnetic field is crucially important for understanding long-term field evolution and for constraining models of the Earth's dynamo. Paleointensity data are needed to understand how the geomagnetic field reverses its polarity, how and why geomagnetic excursions occur, to understand paleosecular variation, and to constrain models for field generation at all timescales from superchrons ($\sim 10^7$ years) to secular variation (10^2–10^4 years). While variations in the direction of the paleomagnetic vector are well known on a variety of timescales and with a reasonable global distribution, there is a paucity of paleointensity data [e.g., *Perrin and Schnepp*, 2004], which are needed for a full vector representation of the geomagnetic field. Seventy percent of paleointensity data are concentrated in the last 20 Myr, while 35% of the data span the last Myr. We therefore lack a complete description of the geomagnetic field over many timescales, particularly beyond the last million years.

[3] The principal reason for the paucity of reliable absolute paleointensity data is that the method of *Thellier and Thellier* [1959] (hereafter referred to as the Thellier technique), which is the most reliable technique for extracting paleointensities from materials that retain a thermoremanent magnetization (TRM), involves a series of double heatings that are time consuming and that are plagued by a low success rate resulting from thermal alteration of magnetic minerals and nonideal rock magnetic properties. Rocks with ideal magnetic properties will satisfy the three *Thellier* [1938] laws, and, if they do not undergo thermal alteration during the stepwise double heatings, provide an opportunity to obtain a reliable paleointensity determination. These laws are as follows: (1) reciprocity, a partial thermoremanent magnetization (pTRM) acquired between temperatures T_1

[1]National Oceanography Centre, University of Southampton, Southampton, UK.
[2]Now at Institut de Minéralogie et de Physique de la Matière Condensée, Université Pierre et Marie Curie, Paris, France.
[3]Department for Earth and Environmental Sciences, Geophysics Section, Ludwig-Maximilians-Universität München, Munich, Germany.
[4]Laboratoire des Sciences du Climat et de l'Environnement, Unité Mixte CEA-CNRS, Gif-sur-Yvette, France.
[5]Laboratoire Tectonophysique, CNRS and Université Montpellier II, Montpellier, France.

0148-0227/06/2005JB004126$09.00

and T_2 during cooling in an applied field will be thermally demagnetized over precisely this temperature interval when heated in zero field; that is, blocking and unblocking temperatures will be identical; (2) independence, pTRM is independent in direction and intensity of any other pTRM produced over a temperature interval that does not overlap (T_1, T_2) since the grains carrying the two pTRMs represent different parts of the blocking temperature (T_B) spectrum; and (3) additivity, pTRMs produced by the same applied field have intensities that are additive because the T_B spectrum can be decomposed into nonoverlapping fractions, each associated with their own pTRM.

[4] None of the three *Thellier* [1938] laws will apply if the strength of magnetostatic interactions among the magnetic particles (H_{int}) exceeds the strength of the laboratory field H_{lab} used in the paleointensity experiment. The presence of interacting single-domain (SD) particles with different T_B means that pTRMs with nonoverlapping T_B ranges will magnetostatically interact. These pTRMs will therefore not be independent or additive. Significant magnetostatic interactions are therefore likely to give rise to nonlinearity in the Arai diagrams [*Nagata et al.*, 1963] that are used to evaluate paleointensity data. The most commonly used method for determining the presence of magnetostatic interactions in rock magnetism [*Cisowski*, 1981] is, unfortunately, incapable of discriminating between interactions and non-SD behavior. More robust techniques are therefore needed to determine the effects of interactions on paleointensity experiments. Non-SD behavior can also compromise Thellier experiments because multidomain (MD) grains do not obey the three *Thellier* [1938] laws. Reciprocity is not a feature of MD pTRMs because a pTRM with a given T_B will have a distribution of unblocking temperatures instead of a single unblocking temperature. Different MD pTRMs cannot be independent since their unblocking temperature ranges overlap. Additivity is also unlikely because the various MD pTRMs are not independent of each other. Therefore the presence of MD grains leads to a curved Arai plot [*Levi*, 1977; *Dunlop and Xu*, 1994; *Dunlop et al.*, 2005].

[5] Several efforts have been made to provide rock magnetic tests to screen for ideal and nonideal magnetic properties to optimize success rates in paleointensity studies [e.g., *Thomas*, 1993; *Cui et al.*, 1997; *Perrin*, 1998]. However, most rock magnetic parameters are highly ambiguous when obtained from materials containing mixtures of different magnetic grains. In such cases, results provide a weighted average of the components present in the sample [e.g., *Roberts et al.*, 1995; *Carter-Stiglitz et al.*, 2001]. Ideally, a screening technique must discriminate between the magnetic components in the sample, including the degree of magnetostatic interactions.

[6] First-order reversal curve (FORC) diagrams [*Pike et al.*, 1999; *Roberts et al.*, 2000] have been demonstrated to enable discrimination between mixtures of grains with variable magnetic domain states within a sample, and identification of the presence or absence of magnetostatic interactions. This is because grains with different domain structures and interactions plot in different parts of the FORC diagram. The rock magnetic causes of failure to comply with the three *Thellier* [1938] laws in absolute paleointensity experiments (i.e., magnetostatic interactions and non-SD behavior) can be identified using FORC diagrams [*Roberts et al.*, 2000]. In principle, interaction fields weaker than H_{lab} would not be expected to cause failure of the experiment. By quantifying interaction field strengths using the parameters of *Pike et al.* [1999] and *Muxworthy and Dunlop* [2002], it should be possible to empirically determine a threshold strength for interaction fields that would cause failure of the paleointensity experiment. It is worth noting that *Pike et al.* [1999] presented a sensitivity test by comparing estimates of interaction field strength using FORC diagrams compared to the standard ΔM method used in research related to magnetic recording media. They found that FORC diagrams are three times more sensitive in determining interactions. This underscores the potential value of FORC diagrams in paleointensity studies. The present study is aimed at using FORC diagrams to develop prescreening criteria for sample selection in absolute paleointensity studies. The Thellier method is time consuming and can have low success rates, so procedures that can increase efficiency by eliminating samples that are unlikely to give useful paleointensity results could be beneficial. Automated FORC measurements can be performed with sufficient efficiency for this purpose. Other rock magnetic measurements have also been made in this study in case they are useful for supplementing selection criteria based on FORC diagrams.

2. FORC Diagrams

[7] FORC diagrams are constructed by measuring a large number of partial magnetic hysteresis curves known as first-order reversal curves or FORCs [*Pike et al.*, 1999; *Roberts et al.*, 2000]. Starting at positive saturation, the applied field is decreased until a specified reversal field (H_r) is reached. A FORC is the magnetization curve measured at regular field steps from H_r back up to positive saturation. Typically, a large number of FORCs is measured, so that the FORCs fill the interior of a major hysteresis loop (Figure 1a). The magnetization (M) on the FORC with reversal field H_r is denoted by $M(H_r, H)$. The FORC distribution is defined as the mixed second derivative:

$$\rho(H_r, H) \equiv -\frac{\partial^2 M(H_r, H)}{\partial H_r \partial H},$$

which is well defined for $H > H_r$.

[8] When plotting a FORC distribution on a FORC diagram, it is convenient to change coordinates from $\{H_r, H\}$ to $H_c = (H - H_r)/2$ and $H_i = (H + H_r)/2$. Since $\rho(H_r, H)$ is only well-defined for $H > H_r$, a FORC diagram is only well-defined for $H_c > 0$. The FORC distribution is determined at each point by fitting a mixed second-order polynomial of the form $a_1 + a_2 H_A + a_3 H_A^2 + a_4 H_B + a_5 H_B^2 + a_6 H_A H_B$ to a local, moving grid. $\rho(H_A, H_B)$ is equal to the fitted parameter $-a_6$. The size of the local area is determined by a user-defined smoothing factor (SF), where the size of the grid is $(2SF + 1)^2$. A more complete explanation of the measurement and construction of FORC diagrams is given by *Muxworthy and Roberts* [2006]. Details of the interpretive framework for FORC diagrams are given by *Pike et al.* [1999] and *Roberts et al.* [2000], with the most complete published descriptions given by

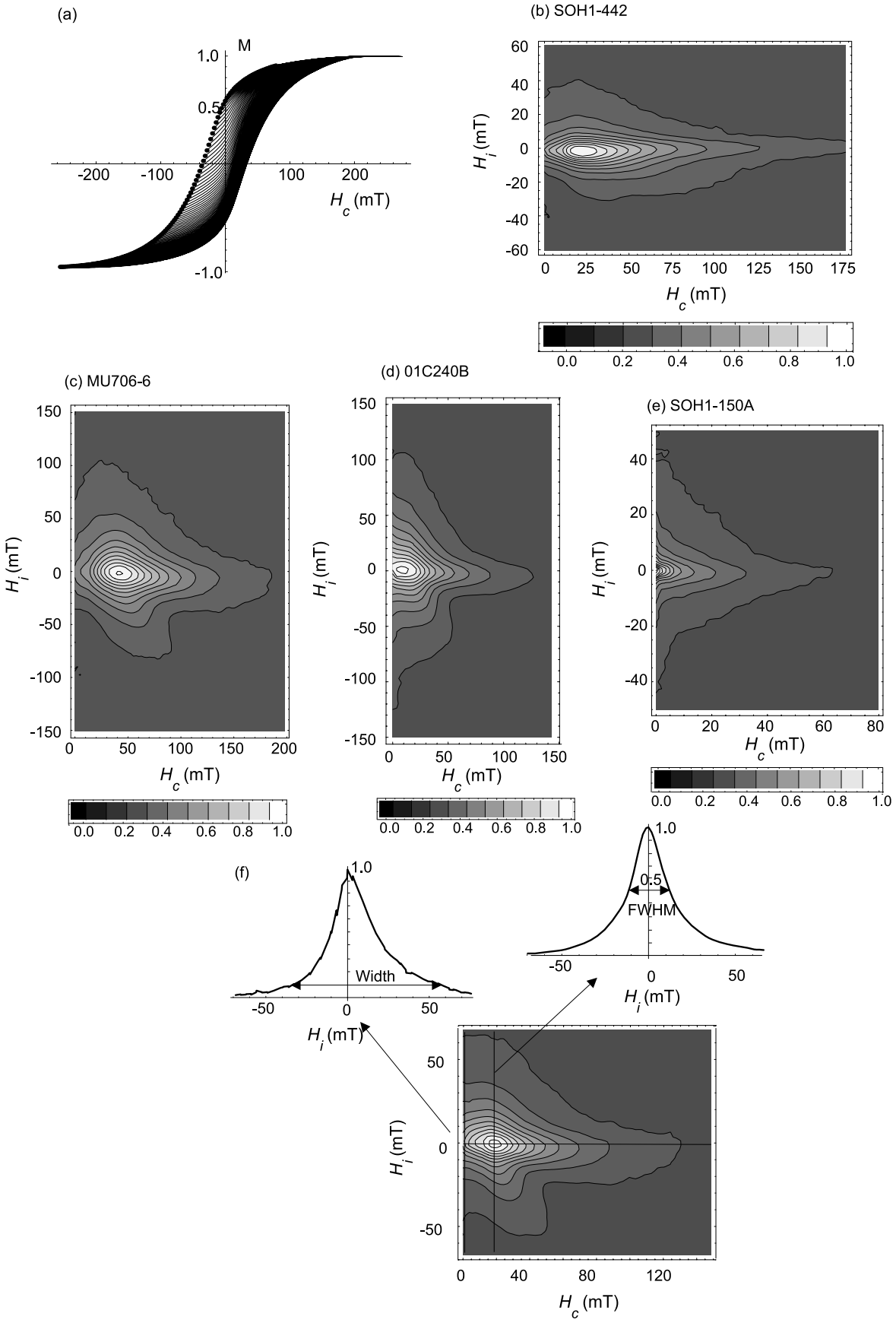
(a)
M
1.0
0.5
-1.0
-200
-100
100
200
H_c (mT)
(b) SOH1-442
H_i (mT)
H_c (mT)
(c) MU706-6
(d) 01C240B
(e) SOH1-150A
(f)
Width
FWHM

Figure 1

Pike et al. [2001a] and *Muxworthy and Roberts* [2006]. This interpretive framework has been developed through examination of FORC diagrams from well-characterized natural samples, as well as using simulated FORC diagrams from magnetic models. Additional micromagnetic and other modeling has confirmed this framework [*Carvallo et al.*, 2003a, 2004; *Muxworthy and Williams*, 2005]. A cross section of the FORC distribution along the H_c axis is equivalent to the distribution of particle microcoercivities, while a cross section through the peak of the FORC distribution parallel to the H_i axis is equivalent to the distribution of interaction fields [*Pike et al.*, 1999; *Roberts et al.*, 2000; *Carvallo et al.*, 2004].

[9] SD particles are characterized by closed concentric contours about a central peak in the FORC distribution (Figures 1b and 1c). SD particle assemblages with strong magnetic interactions have much greater spread of contours parallel to the H_i axis (Figure 1c) than those with less significant interactions (Figure 1b). MD particle systems have markedly different FORC distributions compared to SD systems. For materials with large grains and strong domain wall pinning (e.g., transformer steel), the FORC distribution has nearly vertical contours with the peak close to $H_c = 0$ [*Pike et al.*, 2001a]. Smaller MD particles have less steep contours that intersect the H_i axis (Figure 1d). The inclined contours are probably due to magnetic interactions among domain walls. Smaller MD particles have less divergent contours. Finally, at the other end of the grain size spectrum, fine-grained SD particles undergo varying degrees of thermal relaxation depending on the distribution of grain volumes. The effect is to shift a SD FORC distribution to lower coercivities (Figure 1e), so that the FORC distribution intersects the H_i axis [*Pike et al.*, 2001b]. The fact that superparamagnetic (SP) particles have a manifestation on the FORC diagram reflects the rapid measurement time, which is faster than the relaxation time of the particles. Even though MD and SP particles have distributions centered about the origin of a FORC diagram, the two types of particles have different FORC distributions (Figures 1d and 1e) [*Pike et al.*, 2001a, 2001b] and can also be readily discriminated using low-temperature measurements (where the FORC distribution for SP particles will move to higher coercivities compared to a room temperature measurement, which will not be the case for MD particles). FORC diagrams therefore have considerable potential for detecting the rock magnetic causes of failure of paleointensity experiments.

3. Paleointensity Selection Criteria

[10] This study was performed by measuring FORC diagrams for a large collection of samples for which sister samples have already been subjected to paleointensity analysis. When considering development of rock magnetic criteria for selection of samples for paleointensity analysis, it is equally important to consider the selection criteria used to determine the reliability of paleointensity data. Reliability of paleointensity estimates is judged according to a set of selection criteria, based on Arai [*Nagata et al.*, 1963] and *Zijderveld* [1967] plots. These criteria have progressively evolved over the years [e.g., *Selkin and Tauxe*, 2000].

[11] The samples used in this study come from different laboratories and different measurement methods and selection criteria were used to analyze the results. The two measurement methods used are the original Thellier method [*Thellier and Thellier*, 1959], where the direction of the laboratory field is inverted for the second heating step (i.e., samples are always heated in the presence of a field), and the method modified by *Coe* [1967], where the first heating is in zero field and the second heating is in field. The advantage of the original Thellier method over the *Coe* [1967] method is that it is easier to detect a chemical remanent magnetization (CRM) with unblocking temperatures higher than the chemical transformation temperature in the Zijderveld diagram [*Chauvin et al.*, 1991]. Also, the Thellier method detects reciprocity better than other techniques [*Yu et al.*, 2004]. These disadvantages of the original *Coe* [1967] protocol are overcome by the use of pTRM tail checks, which were used in all presented determinations based on the *Coe* [1967] method.

[12] Consistency in treatment of data from different laboratories is crucial in a study such as this. We have only selected samples that satisfied all of the criteria associated with stability of paleomagnetic directions following *Kissel and Laj* [2004]. We are particularly interested in MD-like behavior on Arai diagrams to test whether FORC diagrams can provide sensitive sample selection criteria.

4. Samples and Methods

[13] In an attempt to develop widely applicable sample selection criteria, we analyzed samples with a broad range of ages, compositions and magnetic carriers, and from a wide range of localities around the world. A recent study used FORC diagrams for a similar purpose, but only 12 samples were analyzed [*Wehland et al.*, 2005]. The more comprehensive nature of the present study makes it more likely to be generally applicable for paleointensity investigations. We measured FORC diagrams for about 200 samples. For each FORC diagram, 120 FORCs were measured using an averaging time of 250 ms. The measurement time for each sample was about 1 hour. Two useful parameters are defined from FORC diagrams for this study. The first is the spread of the FORC distribution along the H_i axis at $H_c = 0$, which is defined as the interval in which the magnitude of the FORC distribution decreases to 10% of its maximum (Figure 1f). We refer to this as the "width" parameter, which reflects the MD contribution to a sample. The second parameter is the full width at half maximum (FWHM) for a profile of the distribution through the coercivity peak parallel to the H_i axis (Figure 1f). This parameter indicates the strength of magnetostatic interac-

Figure 1. Examples of different types of magnetic mineral assemblages identified with FORC diagrams from this study. A sample dominated by (a, b) noninteracting SD grains (SOH1-442; Figure 1a, FORCs; Figure 1b, FORC diagram); (c) interacting SD grains (MU706-6); (d) PSD grains (01C240B); (e) SP grains (SOH1-150A). (f) Definition of the two FORC parameters (width and FWHM) used in this study.

Table 1. Summary of Samples Analyzed in This Study

Sample	Location	Age	Lithology	Successful Samples	Failed Samples	Method	Laboratory	Reference
SOH1	Hawaii	20–120 kyr	tholeiite	29	20	Thellier	Gif-sur-Yvette	*Teanby et al.* [2002]
SOH4	Hawaii	0–100 kyr	tholeiite	22	18	Thellier	Gif-sur-Yvette	*Laj et al.* [2002]
HSDP	Hawaii	0–420 kyr	tholeiite	12	18	Thellier	Gif-sur-Yvette	*Laj and Kissel* [1999]
98C	Amsterdam Island	9–41 kyr	tholeiite	6	2	Thellier	Montpellier	*Carvallo et al.* [2003b]
92M	Lesotho	180 Ma	tholeiite	0	9	Thellier	Montpellier	*Kosterov et al.* [1997]
01C	Mexico	7–11 Ma	andesitic basalt	1	12	Thellier	Montpellier	
	São Tomé	1–5 Ma	alkali basalt	10	9	Coe	Munich	
	Nazca	1.5 kyr	potsherds	8	0	Coe	Munich	
	Tenerife	6 Ma	alkali basalt	2	5	Coe	Munich	*Leonhardt and Soffel* [2006]
	Hawaii	1 Ma	tholeiite	0	6	Coe	Munich	
	Brazil	3 Ma	alkali basalts	2	0	Coe	Munich	*Leonhardt et al.* [2003]

tions within a sample. It should be noted that the FORC distribution is least rigorously calculated along the $H_c = 0$ axis because data cannot be obtained for $H_c < 0$, so the smoothing associated with the polynomial used to calculate the FORC distribution must be relaxed near $H_c = 0$ [*Roberts et al.*, 2000]. Despite possible distortion of the FORC distribution in this part of the FORC diagram, we have preferred to define the width parameter here (Figure 1f) because it best captures the vertical spread of contours associated with MD particles.

[14] Half of the analyzed samples are from the Hawaiian Scientific Drilling Project (HSDP) and Scientific Observation Hole (SOH) numbers 1 and 4 on Kilauea volcano, Hawaii. Paleointensity analyses were performed on SOH1 samples by *Teanby et al.* [2002], with a 70% success rate. SOH4 basalts also gave good paleointensity results, with a 40% success rate [*Laj et al.*, 2002]. Both SOH cores cover the last 100 kyr. The HSDP core spans the last 420 kyr and was drilled in the Mauna Loa and Mauna Kea volcanic series. Paleointensity measurements for the HSDP core had a 75% success rate [*Laj and Kissel*, 1999]. The paleointensity results from the three cores together with paleodirection determinations, carried out at the Laboratoire des Sciences du Climat et de l'Environnement paleomagnetic laboratory in Gif-sur-Yvette, France, allowed detailed analysis of geomagnetic field behavior for the 0–420 kyr time interval.

[15] Further samples analyzed in this study were collected from localities around the world from rocks and potsherds of a wide range of ages (Table 1). Samples were subjected to absolute paleointensity analysis in the paleomagnetic laboratories of the Ludwig-Maximilians University, Munich, Germany, and of the University of Montpellier, France. Paleointensity determinations for the samples analyzed in Munich included pTRM tail checks as well as additivity checks [*Krása et al.*, 2003] in order to detect MD behavior by checking the validity of Thellier's law of additivity. The combination of pTRM checks and additivity checks allows discrimination between magnetic mineral alteration and MD bias, therefore the alteration correction of *Valet et al.* [1996] can be applied in appropriate cases [*Leonhardt et al.*, 2003]. However, MD behavior identified at high temperature could also be a product of thermal alteration, and might not indicate the domain structure of the original magnetic carrier, which is what matters for a correct paleointensity determination. Any alteration corrections must therefore be applied with care. The paleointensity results were analyzed using the ThellierTool software of *Leonhardt et al.* [2004]. The other samples analyzed in this study are described below in the following sections. The results described below are organized according to different relationships observed in FORC diagrams and Arai plots regardless of sample locality and age.

5. Paleointensity Data and FORC Diagrams

5.1. Clear Correlation Between Paleointensity Results and FORC Diagrams

[16] Basalt samples from Mexico have a consistent trend between Arai plots and FORC diagrams. We analyzed 13 samples from the early eruptive stage of the Trans-Mexican Volcanic Belt. The lavas erupted between 11 and 7 Ma and were sampled from the Pacific coast to the longitude of Mexico City, to the north of the modern volcanic arc [*Ferrari et al.*, 1999]. Paleointensity determinations were made using the Thellier method. The resulting Arai plots are all more or less concave-curved (Figure 2). According to the criteria of *Selkin and Tauxe* [2000], the least curved Arai plot still provides a reliable paleointensity estimate. The lines shown on the Arai plots do not represent the fits used to estimate the paleofield intensity. Rather, they connect the first and the last data points on the plots in order to aid visualization of the curvature of the Arai plots.

[17] FORC diagrams range from being SD-like, with closed inner contours and little spread along the H_i axis (Figure 2a), to being more MD-like, with progressively much larger spread of the outer contours, less closed inner contours, and a smaller tail toward high coercivities (Figure 2d). However, the coercivities associated with the peaks of the FORC distributions do not vary significantly. The amount of curvature of the outer contours clearly correlates to the amount of spreading along the $H_c = 0$ axis, which is a measure of the MD contribution to the sample [*Pike et al.*, 2001a]. For the four examples shown in Figure 2, the width of the distribution along the $H_c = 0$ axis (see Figure 1f) increases progressively from 93 to 159 mT. This suggests that the progressively increasing curvature on the Arai plots is a result of increased contributions from MD grains.

[18] The 8 studied samples from Amsterdam Island (Indian Ocean) also have a clear relationship between FORC diagrams and paleointensity behavior. Complete paleointensity results, magnetic properties and radiometric age determinations for the analyzed samples are described by *Carvallo et al.* [2003b]. These samples gave high-quality paleointensity determinations, with a success rate of 50%. Out of the 8 studied samples, 6 gave reliable paleointensity

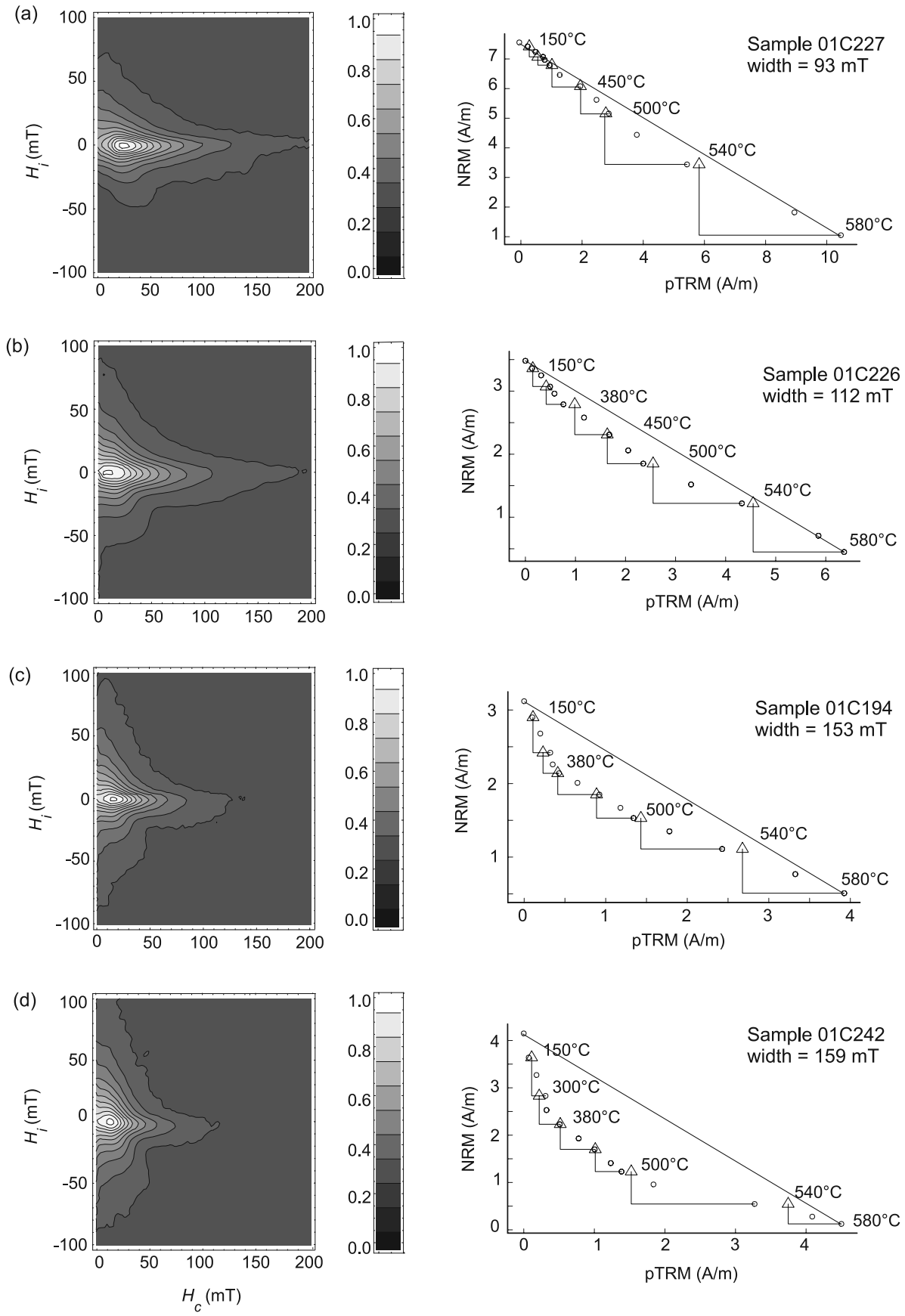
(a)
(b)
(c)
(d)
H_i (mT)
H_c (mT)
NRM (A/m)
pTRM (A/m)
Sample 01C227
width = 93 mT
150°C
450°C
500°C
540°C
580°C
Sample 01C226
width = 112 mT
150°C
380°C
450°C
500°C
540°C
580°C
Sample 01C194
width = 153 mT
150°C
380°C
500°C
540°C
580°C
Sample 01C242
width = 159 mT
150°C
300°C
380°C
500°C
540°C
580°C

Figure 2

determinations. Several differences can be seen between the FORC diagrams for the successful samples (Figure 3a) and those for the unsuccessful samples (Figure 3b). Apart from one sample, which has a FORC distribution with several components, FORC diagrams for the unsuccessful samples are consistently more MD-like than for the successful samples: the width of the distribution is >80 mT for the unsuccessful samples and $\leq$70 mT for the successful samples, the ratio of saturation remanence to saturation magnetization (M_r/M_s) is larger than 0.24 for the successful ones and smaller than 0.23 for the unsuccessful ones, and H_c is greater than 19 mT for the successful samples and smaller than 14 mT for the unsuccessful ones. The FWHM is not so discriminating in this case, which indicates that interactions are probably not a reason for failure of the paleointensity determinations.

[19] Failure of paleointensity experiments for 9 early Jurassic basalt samples from the Mafika Lisiu Pass in Lesotho, southern Africa [*Kosterov et al.*, 1997] can also be explained with FORC diagrams (Figure 3c). During the paleointensity experiment, a significant loss of natural remanent magnetization (NRM) occurs at moderate (200 to 460°C) temperatures, without being accompanied by a proportional increase in TRM acquisition, yielding concave-shaped Arai plots. The FORC diagrams are all similar. There is significant spread of contours along the H_i axis (FWHM between 18 and 35 mT), and the width ranges between 73 and 140 mT, which indicates that the paleointensity experiments failed because of significant magnetostatic interactions and non-SD behavior.

[20] Some of the samples from Hawaii also indicate good agreement between Arai diagrams and FORC diagrams. For example, sample SOH4-177A has ideal behavior on the Arai plot (Figure 3d), with a long linear portion, good pTRM checks and a linear characteristic remanent magnetization component on a Zijderveld diagram. The FORC diagram is consistent with this result: almost all of the contours are closed, spread along the H_i axis is minimal and the negative peak on the H_i axis together indicate the presence of noninteracting SD grains [cf. *Carvallo et al.*, 2004; *Newell*, 2005]. The ideal rock magnetic properties of this sample are clearly consistent with the high-quality paleointensity result. On the other hand, the strongly concave-curved Arai plot for sample SOH4-117B (Figure 3e) is consistent with the large spread of contours on the FORC diagram, which point to MD magnetic carriers, and the large FWHM value indicates significant magnetic interactions.

[21] Arai plots of eight potsherd samples measured at Munich have good linearity. Even though all of the samples have low coercivity (less than 10 mT), the FORC distributions are narrow, with widths less than 35 mT and FWHM values less than 17 mT (Figure 3f). These magnetic properties indicate the dominance of noninteracting SD particles, which are expected to give rise to the observed high-quality Arai plots.

5.2. MD-like Arai Plots With SD-like FORC Diagrams

[22] In contrast to the results presented above, some samples produced discrepancies between the behavior observed on Arai diagrams and FORC diagrams. In some cases, samples with concave-curved Arai plots yielded SD-like FORC diagrams. In the three examples shown in Figure 4, the curvature of the Arai plot is so strong that reliable paleointensity determinations could not be obtained. However, the closed inner contours on the FORC diagrams point to the dominance of SD grains. The Zijderveld diagram for sample SOH4-135A (Figure 4b) is quite curved, which might cause the curvature of Arai plot and explain the discrepancy between the FORC and the Arai plots. The negative region on the H_i axis in the FORC diagram for sample HSDP-56C (Figure 4c) provides further evidence for the presence of SD grains in this sample [cf. *Carvallo et al.*, 2004; *Newell*, 2005]. This negative feature is caused by the decrease of $\partial M/\partial H_r$ with decreasing H, which results in a positive mixed derivative value and therefore a negative value for the FORC distribution [*Muxworthy and Roberts*, 2006]. Furthermore, magnetostatic interactions, as indicated by the FWHM values shown in Figure 4, do not appear to be substantial in these samples. Reasons for the discrepancy between these Arai diagrams and FORC diagrams are discussed below.

5.3. SD-like Arai Plots With MD-like FORC Diagrams

[23] We also observed a few cases where samples have linear Arai plots and MD-like FORC diagrams (Figure 5). Even though sample HSDP-28C (Figure 5a) gave reliable paleointensity determinations, the FORC diagram has no closed contours and a coercivity peak that is close to the vertical axis. Sample MU606-6 also yielded a good paleointensity result, but this is not consistent with the significant vertical spread of the FORC distribution (FWHM = 28.9 mT) through its maximum (Figure 5b). Reasons for these discrepancies are discussed below.

6. Discussion

6.1. Arai Diagram Curvature and Thermal Alteration

[24] In order to test whether the apparent discrepancy between SD-like FORC diagrams and concave-curved Arai plots can be attributed to thermal alteration, we heated some of the Hawaiian samples to 580°C and then remeasured FORC diagrams. For almost all of the samples, there is no difference between the FORC diagrams before or after heating. For example, samples SOH4-135A and SOH1-54A (Figures 6a and 6b) have identical FORC diagrams after two heatings (even after three heatings for sample SOH1-54A). This indicates that either the sample did not alter during the paleointensity experiment, or that alteration resulted from the cumulative effects of more than 2 or 3 heatings. In support of this possibility, sample HSDP-56C (Figure 6c) has apparently undergone alteration during

Figure 2. (left) FORC diagrams and (right) Arai diagrams for four samples from Mexico that demonstrate progressively increasing contributions from MD grains. Samples (a) 01C227; (b) 01C226; (c) 01C194; and (d) 01C242. The line connecting the first and the last data points on the Arai diagrams are shown for reference to aid visualization of the curvature defined by the data in the plots. Triangles represent the pTRM checks. Only sample 01C227 yielded a reliable paleointensity estimate between 150 and 540°C.

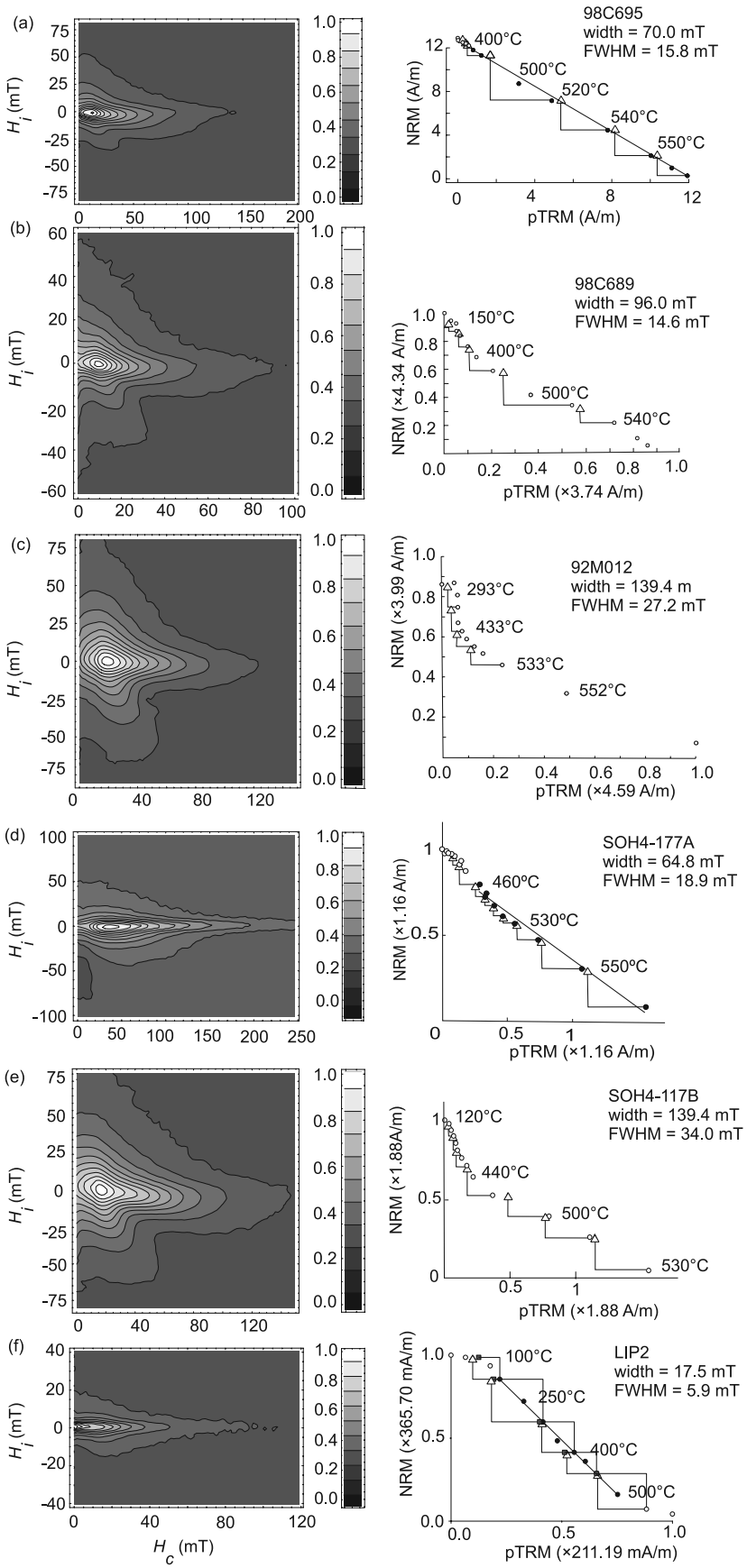
(a)
98C695
width = 70.0 mT
FWHM = 15.8 mT
400°C
500°C
520°C
540°C
550°C
NRM (A/m)
pTRM (A/m)
(b)
98C689
width = 96.0 mT
FWHM = 14.6 mT
150°C
400°C
500°C
540°C
NRM (×4.34 A/m)
pTRM (×3.74 A/m)
(c)
92M012
width = 139.4 m
FWHM = 27.2 mT
293°C
433°C
533°C
552°C
NRM (×3.99 A/m)
pTRM (×4.59 A/m)
(d)
SOH4-177A
width = 64.8 mT
FWHM = 18.9 mT
460ºC
530ºC
550ºC
NRM (×1.16 A/m)
pTRM (×1.16 A/m)
(e)
SOH4-117B
width = 139.4 mT
FWHM = 34.0 mT
120°C
440°C
500°C
530°C
NRM (×1.88A/m)
pTRM (×1.88 A/m)
(f)
LIP2
width = 17.5 mT
FWHM = 5.9 mT
100°C
250°C
400°C
500°C
NRM (×365.70 mA/m)
pTRM (×211.19 mA/m)
H_i (mT)
H_c (mT)

Figure 3

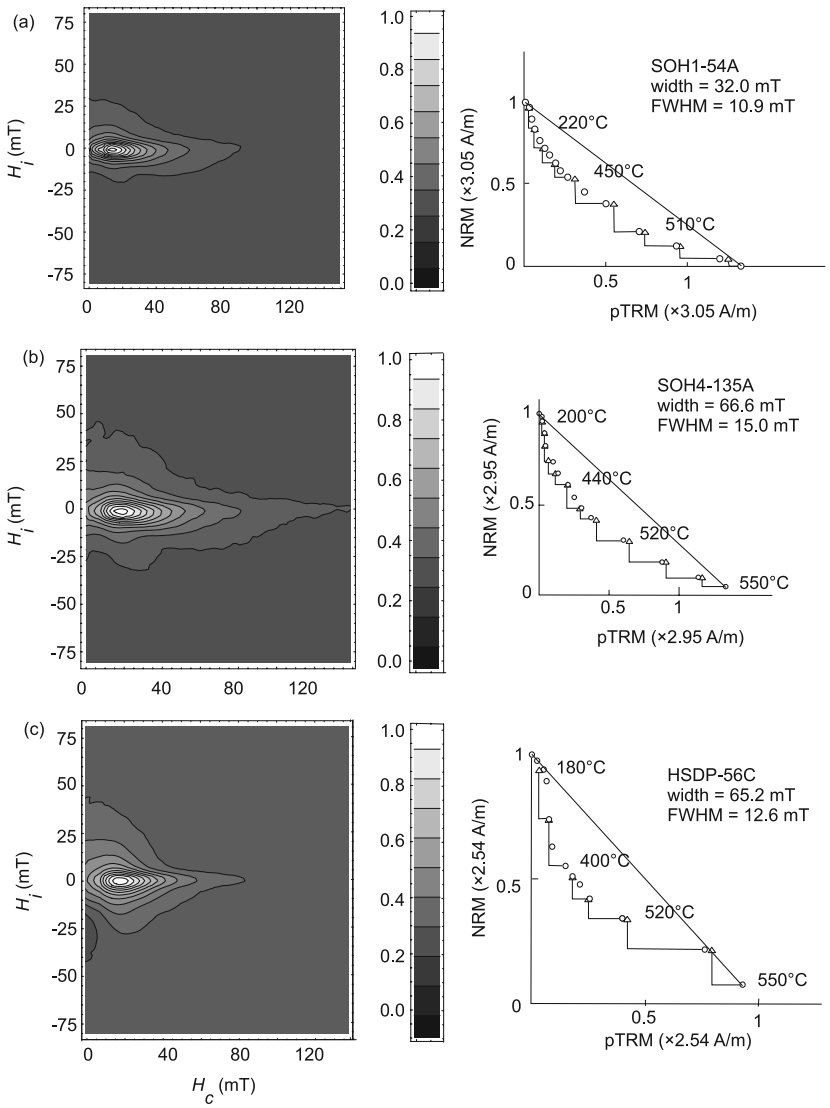

Figure 4. (left) FORC diagrams and (right) Arai diagrams for samples with SD-like FORC diagrams and MD-like Arai diagrams. (a) Sample SOH1-54A (Hawaii); (b) sample SOH4-135A (Hawaii); and (c) sample HSDP-56C (Hawaii). On the Arai plots, triangles represent the pTRM checks. None of them yielded a reliable paleointensity estimate. The line connects the first and the last data points to aid visualization of the curvature of the Arai plot.

heating: the FORC distribution becomes more contracted along both axes after progressive heating and the negative peak that is evident in the pristine sample has almost disappeared after the second heating.

[25] In addition to analyzing samples that yielded concave-curved Arai diagrams to test the effects of thermal alteration, we also heated and remeasured some samples for which the Arai plots indicate evidence of thermal alteration. However, the FORC diagrams after heating are similar to those before heating. This result indicates that thermal alteration is difficult to detect with only a few heatings. In some cases alteration occurs after only one heating, but in other cases it occurs after repeated heatings. The likelihood of thermal alteration during the paleointensity experiment is often assessed by examining the reversibility of $M_s(T)$ curves, usually up to the Curie point. However, some samples might alter at higher temperatures, but not at a lower temperature range that would still give a reliable

Figure 3. (left) FORC diagrams and (right) Arai diagrams for samples with consistent behavior on the two diagrams. (a) Sample 98C695 (Amsterdam Island); (b) sample 98C689 (Amsterdam Island); (c) sample 92M012 (Lesotho); (d) sample SOH4-177A (Hawaii); (e) sample SOH4-117B (Hawaii); and (f) sample LIP2 (Nazca). On the Arai plots, triangles represent pTRM checks, and solid squares represent the pTRM tail checks on Figure 3f. The line on Figures 3a, 3d, and 3f represent the best fits used for paleointensity estimates, the solid (open) symbols correspond to accepted (rejected) points. The other samples did not yield reliable paleointensity results.

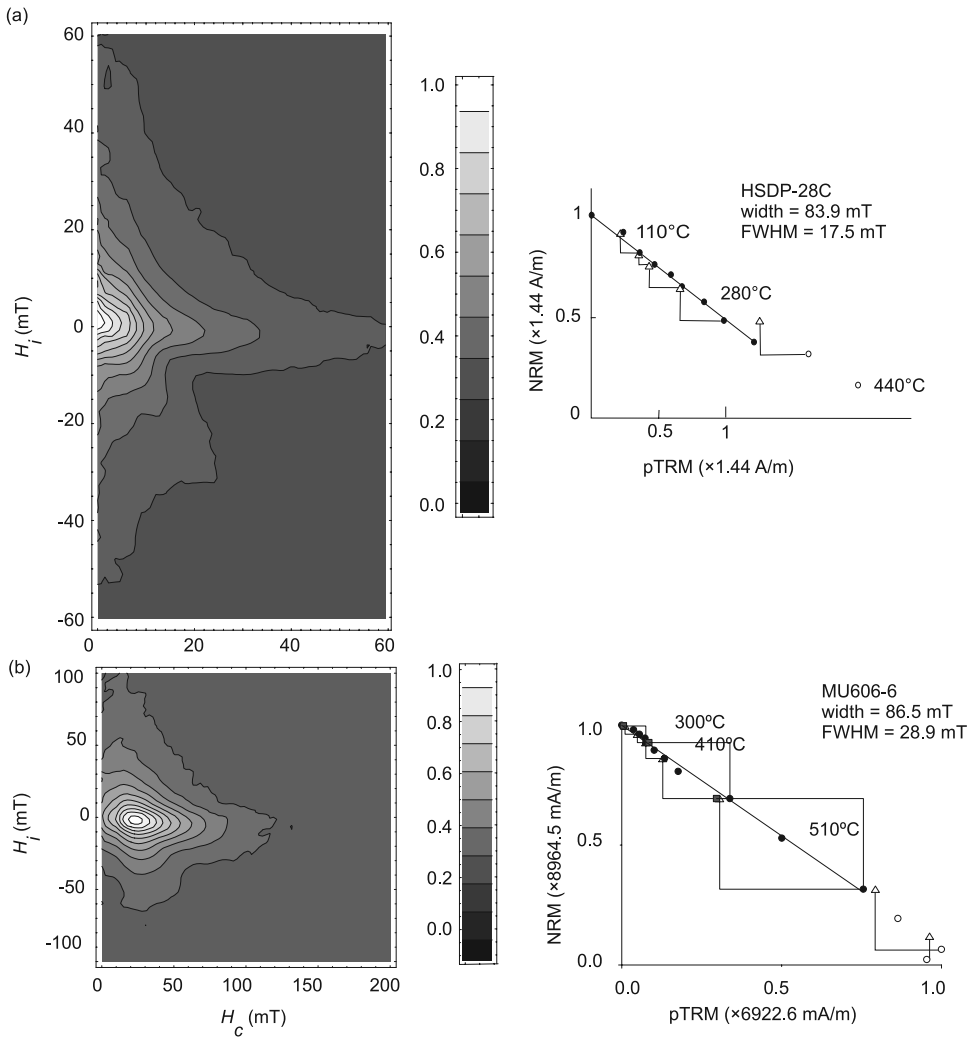

Figure 5. (left) FORC diagrams and (right) Arai diagrams for samples with MD-like FORC diagrams and SD-like Arai diagrams. (a) Sample HSDP-28C (Hawaii) and (b) sample MU606-6 (Brazil). On the Arai plots, triangles represent the pTRM checks, the lines indicate the best fits used for paleointensity estimates, and the solid (open) symbols correspond to accepted (rejected) data points.

paleointensity determination. Also, as we have shown here, alteration might occur after more than one heating. These factors make it practically difficult to test for thermal alteration.

[26] Another way of checking for thermal alteration is by measuring a FORC diagram after a sample has been analyzed in a paleointensity experiment since this is the sample that has undergone heating at multiple steps. FORC diagrams for 5 such samples from the HSDP core are markedly different from the FORC diagrams for the unheated twin samples, which indicates that thermal alteration has occurred. Sample HSDP-56C (Figure 6c) is a typical example: the FORC distribution after completion of the paleointensity experiment is expanded along both axes. The extent of the alteration is much more marked in the multiply heated sample than after only one or two heatings. Thermal alteration could therefore be the cause of the curvature of some Arai plots despite the SD-like magnetic properties indicated by FORC diagrams for some samples (Figure 4). Unfortunately, only a small number of heated samples were available after completion of paleointensity analysis, so we could not systematically check for thermal alteration after the paleointensity measurement.

6.2. Sample Selection Criteria Based on FORC Diagrams

[27] Hysteresis parameters (e.g., M_{rs}/M_s and the ratio of the coercivity of remanence over the coercivity H_{cr}/H_c) are often used to characterize domain structure. We have found that the parameters FWHM and width associated with the FORC distribution, as well as the coercive force H_c, are much more discriminating parameters than standard hysteresis parameters represented on a Day plot [*Day et al.*, 1977] (Figure 7). Successful samples should have large H_c, small width and small FWHM, to approximate ideal noninteracting SD magnetic properties. However, parts of the distributions of these three parameters overlap for samples that yielded successful and unsuccessful paleointensity results. This overlap partially results from the fact that magnetically ideal samples failed to produce high-quality paleointensity results because of thermal alteration. However, the average

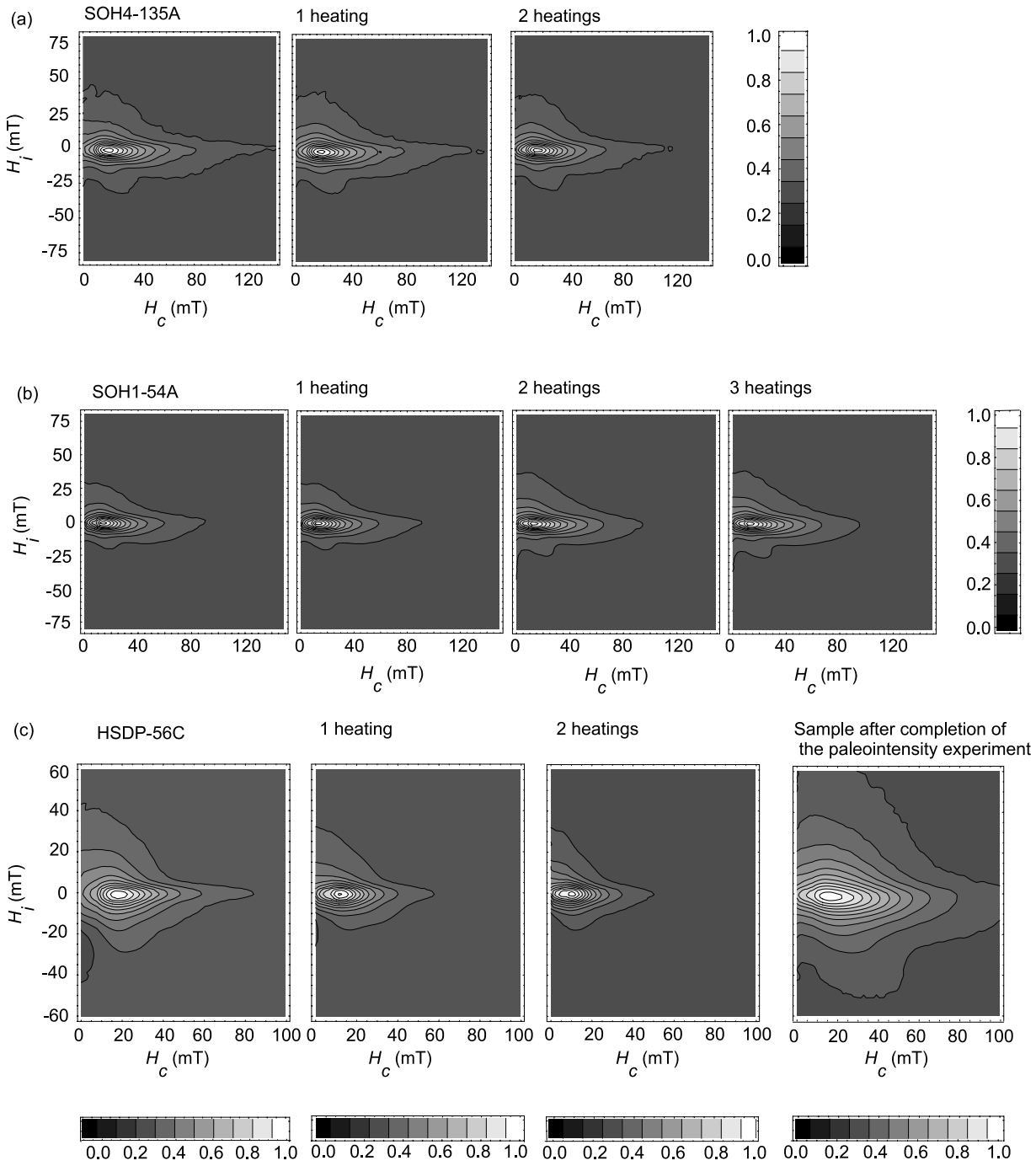

Figure 6. FORC diagrams measured at room temperature prior to any thermal treatment and after heating for 20 min at 580°C. (a) Sample SOH4-135A; (b) sample SOH1-54A; and (c) FORC diagrams measured at room temperature prior to heating, after heating for 20 min at 580°C and after the full paleointensity experiment for sample HSDP-56C.

width of the FORC distribution for failed samples (86.1 mT) is higher than that of the successful samples (79.1 mT). The average FWHM is also slightly higher for the failed samples compared to the successful samples (20.2 mT compared to 18.6 mT). Finally, the average H_c is only slightly lower for the failed (18.2 mT) compared to the successful (19.5 mT) samples.

[28] Statistically, the FWHM, width and H_c distributions for successful and unsuccessful samples are not distinct. However, only one third of the unsuccessful samples failed the paleointensity experiment because of nonideal grain size or because of magnetic interactions. Two thirds of the samples failed because of thermal alteration, therefore statistics are not useful for assessing the distinctness of our parameters.

[29] However, in order to use FORC diagrams to develop criteria for sample selection in paleointensity studies, we need to set threshold values on these three parameters.

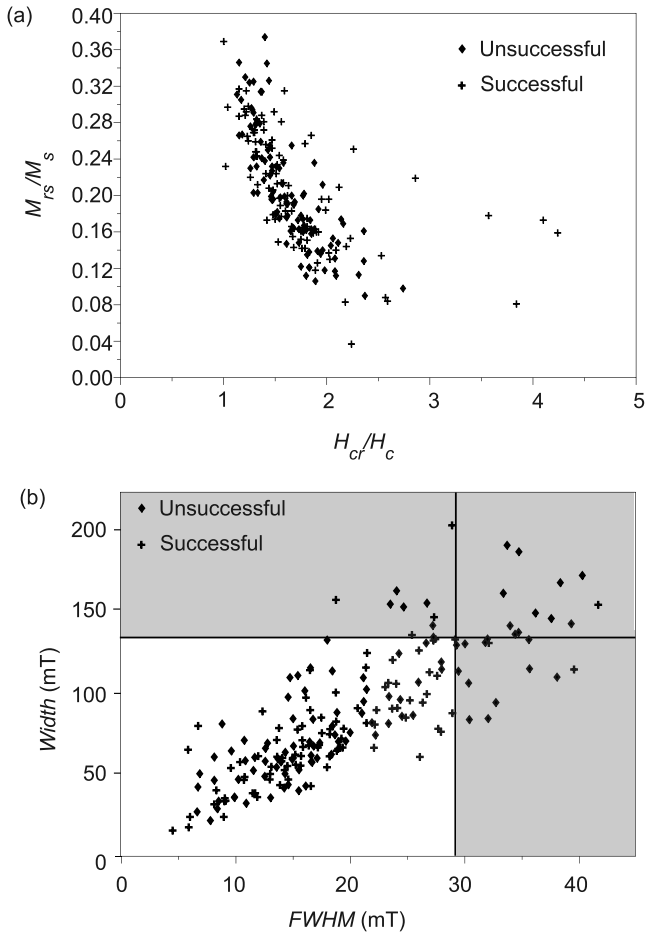

Figure 7. (a) M_{rs}/M_s versus H_{cr}/H_c (Day plot) for the studied samples; (b) FWHM versus width parameter for the same samples. Crosses indicate samples that yielded successful paleointensity results; diamonds indicate samples that yielded unsuccessful paleointensity results. The lines indicate the threshold values for the two parameters. The samples that fall in the gray area are eliminated according to these selection criteria.

Because of the overlap in values for samples that yielded successful and unsuccessful results, the combination of these values must allow us to reject as many failed samples as possible without rejecting too many reliable samples. The values of the thresholds for the selection criteria depend on the acceptability of losing reliable samples. We used FWHM and width threshold values that minimize the number of reliable samples that would be rejected. Using threshold values of FWHM = 29 mT and width = 132 mT, 29 failed samples are eliminated (Figure 7b). By adding a limiting threshold on H_c at 5.4 mT, another 3 samples can be eliminated. Overall, 32% of the failed samples would be rejected using these three threshold values. However, 5 samples from Hawaii (SOH1-008A, SOH1-008B, SOH1-040A, SOH4-101C, and SOH4-122C), and 2 from Sao Tome (MU722-6 and MU723-5) that were accepted as giving reliable paleointensity estimates would also be rejected using these criteria. Even though these 7 samples pass the paleointensity selection criteria of *Selkin and Tauxe* [2000] and *Kissel and Laj* [2004] (linearity of the Arai and Zijderveld plots, a large enough fraction f of the NRM destroyed on the NRM/TRM segment that is chosen to define the paleointensity factor, and acceptable pTRM checks), most of these samples do not represent ideal paleointensity determinations (Figure 8). For example, samples SOH4-122C and MU722-6 are slightly concave curved. The same number of rejected samples is achieved when the width is between 130 and 139 mT, with FWHM being kept constant. Alternatively, the same rejection rate is achieved for FWHM values between 28.9 mT and 29.5 mT for the same width.

[30] We tried to base our study on a variety of samples with variable magnetic mineralogy, in order to provide criteria that would be generally applicable. However, it is probably possible to refine the criteria by taking into account the magnetic mineralogy, using parameters such as the Curie temperature. Our data set, although quite large for a general study, was too small to carry out such a detailed analysis. We also did not have Curie temperature data for all samples.

6.3. Other Sample Selection Criteria Not Based on FORC Diagrams

[31] While paleomagnetic records of the ancient geomagnetic field represent a low-field magnetization, FORC diagrams are high-field measurements. A sample containing a mixture of different populations of magnetic grains could therefore conceivably respond differently in high-field or in low-field measurements. The alternating field (AF) demagnetization spectrum can be used to characterize the magnetization carriers in low fields, which provides a useful comparison with high-field FORC measurements. The coercivity spectrum for SD grains will be S-shaped where there is an initial plateau with negligible demagnetization and an inflexion point at intermediate fields; the coercivity spectrum changes to an exponential decay curve as grain size increases from the SD to the large MD state [*Dunlop and Özdemir*, 1997]. The median destructive field (MDF) provides a measure of the coercivity. SD grains will have large MDF values, whereas MD grains will have low MDF values.

[32] Whenever we had enough material, a chip of each sample used for FORC measurements was AF demagnetized and the MDF was calculated (89 unsuccessful and 79 successful samples). Even though the MDF distributions of successful and unsuccessful samples overlap, the average MDF for the successful samples is larger than that of unsuccessful samples (36.1 mT compared to 27.3 mT). AF demagnetization spectra can explain some of the discrepancies between FORC diagrams and Arai plots. The 7 reliable samples that would be eliminated with the FORC criteria have SD-like AF demagnetization spectra and high MDFs (between 25 and 70 mT; Figure 9), which suggests that either the presence of interactions or thermal alteration is responsible for the curvature of the Arai plot at high temperatures.

[33] Unfortunately, AF demagnetization data are not available for all of the studied samples, so we cannot use parameters associated with AF demagnetization as additional selection criteria in this study. However, taking into account the data that we have, setting a threshold of MDF = 12.9 mT (instead of the FORC width parameter)

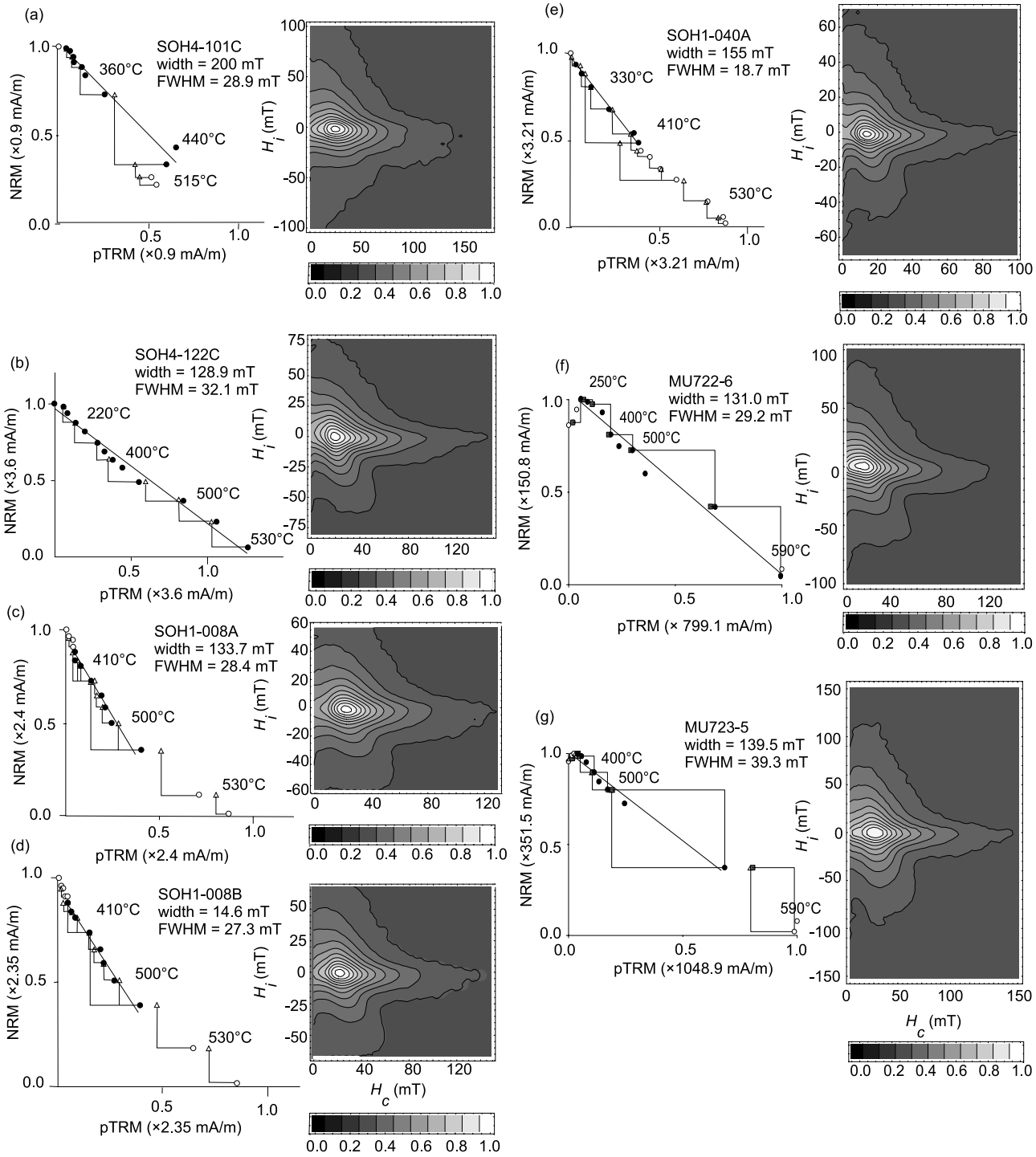

Figure 8. (left) Arai diagrams and (right) FORC diagrams for the seven samples that yielded successful paleointensity determinations but that would be eliminated with the FORC-based sample selection criteria. (a) Sample SOH4-101C; (b) sample SOH4-122C; (c) sample SOH1-008A; (d) sample SOH1-008B; (e) sample SOH1-040A; (f) sample MU722-6; (g) sample MU723-5. On the Arai diagrams, triangles represent the pTRM checks, squares represent the pTRM tail checks, the lines are the best fit lines used for the paleointensity estimates, and the solid (open) symbols correspond to accepted (rejected) points.

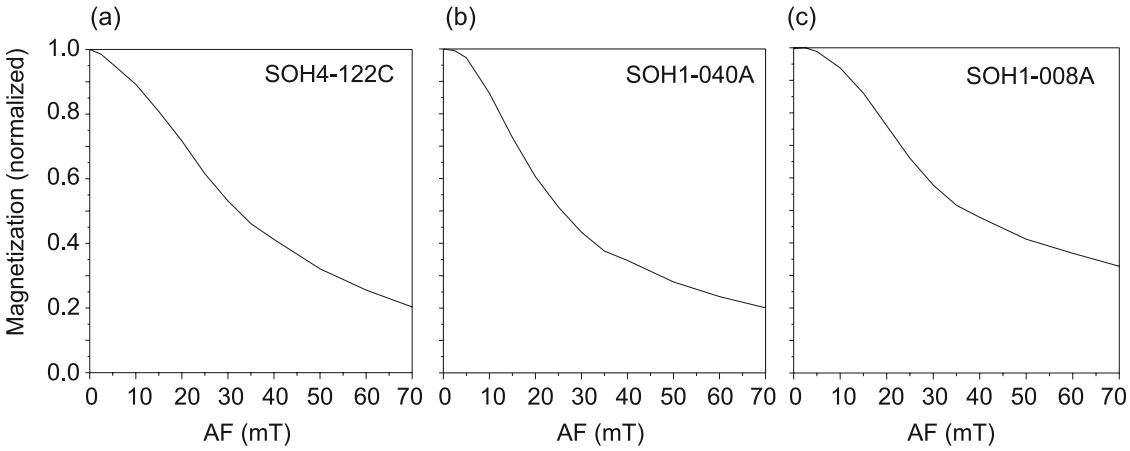

Figure 9. AF demagnetization spectra for three successful samples that would have been rejected with the FORC-based sample selection criteria.

would allow us to reject 20 unsuccessful samples, without rejecting reliable samples, in addition to the 19 that are rejected using the FWHM interaction criterion. Together with the 5 samples rejected using H_c, a total of 43% of unsuccessful samples can be rejected using our preselection criteria, while only rejecting 3 out of 94 reliable samples. The MDF is more discriminating than the FORC distribution width for detecting MD contributions to the low field magnetization (NRM). However, AF demagnetization spectra cannot detect the presence of interactions, so FORC diagrams still represent a critical aspect of our selection criteria.

7. Conclusions

[34] FORC diagrams were measured for 99 unsuccessful and for 92 successful samples used for paleointensity experiments. In general, the FORC diagrams for the successful samples are SD-like with minor to negligible interactions, while FORC diagrams for the unsuccessful samples are more diverse. Unsuccessful samples could have failed the paleointensity criteria because of thermal alteration, which is not detectable on a FORC diagram measured at room temperature.

[35] Selection criteria based on the FWHM of a vertical profile through the maximum of the FORC distribution and on the width of the distribution along the $H_c = 0$ axis, provide a measure of interaction strength and of MD contributions. Setting thresholds at 132 mT for width and 29 mT for FWHM allows maximization of the number of unsuccessful rejected samples and minimization of the number of successful rejected samples. With an additional threshold of $H_c = 5.4$ mT, 32 unsuccessful samples could be rejected. Seven reliable samples (about 8%) would also be rejected using these selection criteria. However, even though they satisfied the paleointensity selection criteria, these ''reliable'' samples did not represent ideal paleointensity determinations (Figure 8).

[36] AF demagnetization spectra and the resultant MDFs provide a measure of the MD contribution that might be more discriminating of their contribution to the NRM than the FORC distribution width at $H_c = 0$. We were unable to measure AF demagnetization spectra for all of our samples, but available data suggest that 43% of the unsuccessful samples can be eliminated (and only 3 reliable samples) if a criterion using a threshold value of 12.9 mT for MDF is used instead of the width of the FORC distribution.

[37] Considering that thermal alteration is a major cause of failure for paleointensity determinations and that it cannot be detected on FORC diagrams measured at room temperature, being able to eliminate at least one third of the unsuccessful samples with nonideal rock magnetic properties (and potentially more than 40% of unsuccessful samples) represents a significant improvement in paleointensity measurement time. It took about one hour to measure each FORC diagram in this study, but it is possible to decrease this time to 30 min for strongly magnetized material such as basalts. The samples that failed because of the presence of interactions or MD behavior are efficiently detected using FORC diagrams. Our sample selection criteria therefore appear to have considerable promise for increasing the efficiency of absolute paleointensity studies.

[38] **Acknowledgments.** This research was funded by Marie Curie EC contract MCIF-CT-2004-0107843. We thank Jeff Gee and Ken Kodama for constructive review comments that helped to improve the paper.

References

Carter-Stiglitz, B., B. Moskowitz, and M. Jackson (2001), Unmixing magnetic assemblages and the magnetic behavior of bimodal mixtures, *J. Geophys. Res.*, *106*, 26,397–26,411.

Carvallo, C., A. R. Muxworthy, D. J. Dunlop, and W. Williams (2003a), Micromagnetic modeling of first-order reversal curve (FORC) diagrams for single-domain and pseudo-single-domain magnetite, *Earth Planet. Sci. Lett.*, *213*, 375–390.

Carvallo, C., P. Camps, G. Ruffet, B. Henry, and T. Poidras (2003b), Mono Lake or Laschamps geomagnetic event recorded from lava flows in Amsterdam Island (southeastern Indian Ocean), *Geophys. J. Int.*, *154*, 767–782.

Carvallo, C., Ö. Özdemir, and D. J. Dunlop (2004), First-order reversal curve (FORC) diagrams of elongated single-domain grains at high and low temperatures, *J. Geophys. Res.*, *109*, B04105, doi:10.1029/2003JB002539.

Chauvin, A., P. Y. Gillot, and N. Bonhommet (1991), Paleointensity of the Earth's magnetic field recorded by two late Quaternary volcanic sequences at the island of La Reunion (Indian Ocean), *J. Geophys. Res.*, *96*, 1981–2006.

Cisowski, S. (1981), Interacting vs. non-interacting domain behavior in natural and synthetic samples, *Phys. Earth Planet. Inter.*, *26*, 56–62.

Coe, R. S. (1967), The determination of paleointensities of the Earth's magnetic field with emphasis on mechanisms which could cause non-

ideal behavior in Thellier's method, *J. Geomagn. Geoelectr.*, *19*, 157–179.
Cui, Y. L., K. L. Verosub, A. P. Roberts, and M. Kovacheva (1997), Mineral magnetic criteria for sample selection in archaeomagnetic studies, *J. Geomagn. Geoelectr.*, *49*, 567–585.
Day, R., M. Fuller, and V. A. Schmidt (1977), Hysteresis properties of titanomagnetites: Grain size and composition dependence, *Phys. Earth Planet. Inter.*, *13*, 260–267.
Dunlop, D. J., and Ö. Özdemir (1997), *Rock Magnetism: Fundamentals and Frontiers*, 573 pp., Cambridge Univ. Press, New York.
Dunlop, D. J., and S. Xu (1994), Theory of partial thermoremanent magnetization in multidomain grains: 1. Repeated identical barriers to wall motion (single microcoercivity), *J. Geophys. Res.*, *99*, 9005–9023.
Dunlop, D. J., B. Zhang, and Ö. Özdemir (2005), Linear and non-linear Thellier paleointensity behavior of natural minerals, *J. Geophys. Res.*, *110*, B01103, doi:10.1029/2004JB003095.
Ferrari, L., M. Lopez-Martinez, G. Aguirre Diaz, and G. Carrasco Nunez (1999), Space-time patterns of Cenozoic arc volcanism in central Mexico: From the Sierra Madre Occidental to the Mexican volcanic belt, *Geology*, *27*, 303–306.
Kissel, C., and C. Laj (2004), Improvements in procedure and paleointensity selection criteria (PICRIT-03) for Thellier and Thellier determinations: Applications to Hawaiian basaltic long cores, *Phys. Earth Planet. Inter.*, *147*, 155–169.
Kosterov, A. A., M. Prévot, M. Perrin, and V. A. Shashkanov (1997), Paleointensity of the Earth's magnetic field in the Jurassic: New results from a Thellier study of the Lesotho Basalt, southern Africa, *J. Geophys. Res.*, *102*, 24,859–24,872.
Krása, D., C. Heunemann, R. Leonhardt, and N. Petersen (2003), Experimental procedure to detect multidomain remanence during Thellier-Thellier experiments, *Phys. Chem. Earth*, *28*, 681–687.
Laj, C., and C. Kissel (1999), Geomagnetic field intensity at Hawaii for the last 420 kyr from the Hawaii Scientific Drilling Project Core, Big Island, Hawaii, *J. Geophys. Res.*, *104*, 15,317–15,338.
Laj, C., C. Kissel, V. Scao, J. Beer, D. M. Thomas, H. Guillou, R. Muscheler, and G. Wagner (2002), Geomagnetic intensity and inclination variations at Hawaii for the past 98 kyr from core SOH-4 (Big Island): A new study and a comparison with existing contemporary data, *Phys. Earth Planet. Inter.*, *129*, 205–243.
Leonhardt, R., and H. C. Soffel (2006), The growth, collapse and quiescence of Teno volcano, Tenerife: New constraints from paleomagnetic data, *Int. J. Earth Sci*, in press.
Leonhardt, R., J. Matzka, and E. A. Menor (2003), Absolute paleointensities and paleodirections from Fernando de Noronha, Brazil, *Phys. Earth Planet. Inter.*, *139*, 285–303.
Leonhardt, R., C. Heunemann, and D. Krása (2004), Analyzing absolute paleointensity determinations: Acceptance criteria and the software ThellierTool4.0, *Geochem. Geophys. Geosyst.*, *5*, Q12016, doi:10.1029/2004GC000807.
Levi, S. (1977), The effect of magnetite particle size on paleointensity determinations of the geomagnetic field, *Phys. Earth Planet. Inter.*, *13*, 245–259.
Muxworthy, A. R., and D. J. Dunlop (2002), First-order reversal curve (FORC) diagrams for pseudo-single-domain magnetites at high temperature, *Earth Planet. Sci. Lett.*, *203*, 369–382.
Muxworthy, A. R., and A. P. Roberts (2006), First-order reversal curve (FORC) diagrams, in *Encyclopedia of Geomagnetism and Paleomagnetism*, edited by D. Gubbins, and E. Herrero-Bervera, Springer, New York, in press.
Muxworthy, A. R., and W. Williams (2005), Magnetostatic interaction fields in first-order-reversal-curve (FORC) diagrams, *J. Appl. Phys.*, *97*, 063905.
Nagata, T., Y. Arai, and K. Momose (1963), Secular variation of the geomagnetic total force during the last 5000 years, *J. Geophys. Res.*, *68*, 5277–5281.
Newell, A. J. (2005), A high-precision model of first-order reversal curve (FORC) functions for single-domain ferromagnets with uniaxial anisotropy, *Geochem. Geophys. Geosyst.*, *6*, Q05010, doi:10.1029/2004GC000877.
Perrin, M. (1998), Paleointensity determination, magnetic domain structure, and selection criteria, *J. Geophys. Res.*, *103*, 30,591–30,600.
Perrin, M., and E. Schnepp (2004), IAGA paleointensity database: Distribution and quality of the data set, *Phys. Earth Planet. Inter.*, *147*, 255–267.
Pike, C. R., A. P. Roberts, and K. L. Verosub (1999), Characterizing interactions in fine magnetic particle systems using first order reversal curves, *J. Appl. Phys.*, *85*, 6660–6667.
Pike, C. R., A. P. Roberts, M. J. Dekkers, and K. L. Verosub (2001a), An investigation of multi-domain hysteresis mechanisms using FORC diagrams, *Phys. Earth Planet. Inter.*, *126*, 11–25.
Pike, C. R., A. P. Roberts, and K. L. Verosub (2001b), FORC diagrams and thermal relaxation effects in magnetic particles, *Geophys. J. Int.*, *145*, 721–730.
Roberts, A. P., Y. L. Cui, and K. L. Verosub (1995), Wasp-waisted hysteresis loops: Mineral magnetic characteristics and discrimination of components in mixed magnetic systems, *J. Geophys. Res.*, *100*, 17,909–17,924.
Roberts, A. P., C. R. Pike, and K. L. Verosub (2000), FORC diagrams: A new tool for characterizing the magnetic properties of natural samples, *J. Geophys. Res.*, *105*, 28,461–28,475.
Selkin, P. A., and L. Tauxe (2000), Long-term variations in palaeointensity, *Philos. Trans. R. Soc. London*, *358*, 1065–1088.
Teanby, N., C. Laj, D. Gubbins, and M. Pringle (2002), A detailed paleointensity and inclination record from drill core SOH1 on Hawaii, *Phys. Earth Planet. Inter.*, *131*, 101–140.
Thellier, E. (1938), Sur l'aimantation des terres cuites et ses applications geophysiques, *Ann. Inst. Phys. Globe Univ. Paris*, *16*, 157–302.
Thellier, E., and O. Thellier (1959), Sur l'intensité du champ magnétique terrestre dans la passé historique et géologique, *Ann. Geophys.*, *15*, 285–376.
Thomas, D. N. (1993), An integrated rock magnetic approach to the selection or rejection of ancient basalt samples for palaeointensity experiments, *Phys. Earth Planet. Inter.*, *75*, 329–342.
Valet, J. P., J. Brassart, I. Le Meur, V. Soler, X. Quidelleur, E. Tric, and P. Y. Gillot (1996), Absolute paleointensity and magnetomineralogical changes, *J. Geophys. Res.*, *101*, 25,029–25,055.
Wehland, F., R. Leonhardt, F. Vadeboin, and E. Appel (2005), Magnetic interaction analysis of basaltic samples and pre-selection for absolute palaeointensity measurements, *Geophys. J. Int.*, *162*, 315–320.
Yu, Y., L. Tauxe, and A. Genevey (2004), Toward an optimal geomagnetic field intensity determination technique, *Geochem. Geophys. Geosyst.*, *5*, Q02H07, doi:10.1029/2003GC000630.
Zijderveld, J. D. A. (1967), AC demagnetization of rocks: Analysis of results, in *Methods in Paleomagnetism*, edited by D. W. Collinson, K. M. Creer, and S. K. Runcorn, pp. 254–386, Elsevier, New York.

P. Camps and M. Perrin, Laboratoire Tectonophysique, CNRS and Université Montpellier II, Case 049, F-34095 Montpellier, France.
C. Carvallo, Institut de Minéralogie et de Physique de la Matière Condensée, Université Pierre et Marie Curie, Campus Boucicaut, 140 rue de Lourmel, F-75015 Paris, France. (claire.carvallo@impmc.jussieu.fr)
C. Kissel and C. Laj, Laboratoire des Sciences du Climat et de l'Environnement, Unité Mixte CEA-CNRS, F-91198 Gif-sur-Yvette, France.
R. Leonhardt, Department for Earth and Environmental Sciences, Geophysics Section, Ludwig-Maximilians-Universität München, D-80333 Munich, Germany.
A. P. Roberts, National Oceanography Centre, University of Southampton, European Way, Southampton SO14 3ZH, UK.